PHOTONICS Research

Nonlinear optical performance of few-layer molybdenum diselenide as a slow-saturable absorber

Gaozhong Wang,[1,2,†] Guangxing Liang,[1,†] Aidan A. Baker-Murray,[2] Kangpeng Wang,[2,4] Jing Jing Wang,[2] Xiaoyan Zhang,[3] Daniel Bennett,[2] Jing-Ting Luo,[1,5] Jun Wang,[3] Ping Fan,[1,*] and Werner J. Blau[2]

[1]Shenzhen Key Laboratory of Advanced Thin Films and Applications, College of Physics and Energy, Shenzhen University, Shenzhen 518060, China
[2]School of Physics and the Centre for Research on Adaptive Nanostructures and Nanodevices (CRANN), Trinity College Dublin, Dublin 2, Ireland
[3]Key Laboratory of Materials for High-Power Laser, Shanghai Institute of Optics and Fine Mechanics, Chinese Academy of Sciences, Shanghai 201800, China
[4]e-mail: wangkangpeng@msn.com
[5]e-mail: luojt@szu.edu.cn
*Corresponding author: fanping308@126.com

Received 14 March 2018; revised 16 April 2018; accepted 26 April 2018; posted 27 April 2018 (Doc. ID 325979); published 11 June 2018

Two-dimensional transition metal dichalcogenides are considered promising materials for next-generation photonics and nano-optical devices. Although many previous reports have shown saturable absorption of molybdenum diselenide ($MoSe_2$), these nonlinear optical (NLO) properties of $MoSe_2$ were measured in separate works and under different conditions with their hot-carrier relaxations. Here, we conducted a series of coherent studies on the NLO properties of few-layer $MoSe_2$ via open-aperture Z-scan and degenerate pump-probe techniques. These measurements were taken to test the materials' capabilities as a slow-saturable absorber. A slow-absorber model was employed to analyze the NLO measurements, and the results show that the NLO modulation depth was modeled to be 7.4% and 15.1% for the linear absorption coefficients of 5.22 cm^{-1} and 6.51 cm^{-1}, respectively. The corresponding saturated intensities were modeled to be 39.37 MW/cm^2 and 234.75 MW/cm^2, respectively. The excitation carrier recovery time of few-layer $MoSe_2$ was measured by degenerate pump-probe techniques to be ~220 ps. These nonlinear optical performances make it a promising slow-saturable absorber for passive mode locking in femtosecond lasers.

OCIS codes: (320.7110) Ultrafast nonlinear optics; (190.4400) Nonlinear optics, materials; (160.4330) Nonlinear optical materials; (140.4050) Mode-locked lasers.

https://doi.org/10.1364/PRJ.6.000674

1. INTRODUCTION

Due to their outstanding optical properties, atomically thin, layered crystals of transition metal dichalcogenides (TMDs) provide a fertile playground to investigate intriguing quantum optical phenomena and develop high-performance photonic devices [1–4]. As one important member of TMDs, two-dimensional (2D) molybdenum diselenide ($MoSe_2$) has been experimentally reported for its promising nonlinear optical (NLO) properties in a wide spectral range from visible to near-infrared [5–7], such as giant two-photon absorption, strong nonlinear self-focusing, and nonlinear intensity dependent absorption or scattering, leading to optical limiting [1,8]. In addition, 2D $MoSe_2$ also exhibits strong saturable absorption with a saturated intensity of 590 ± 225 GW/cm^2 and large third-order nonlinear optical susceptibility up to $\sim 1.45 \times 10^{-15}$ esu for 800 nm femtosecond laser pulses [1]. This strong NLO response makes $MoSe_2$ a promising material for a passive mode locker to produce ultrafast pulsed lasers. This application has been demonstrated in a fiber laser and reported femtosecond pulses with a high repetition rate of 3.27 GHz [9]. A saturable absorber can act either as a fast-saturable absorber, i.e., the recovery time is much shorter than the laser pulse duration, or a slow-saturable absorber, i.e., the recovery time is well above the laser pulse duration [10]. However, these papers have not focused on whether few-layer $MoSe_2$ is suitable as a slow-saturable absorber or fast-saturable absorber. The NLO performance of few-layer $MoSe_2$ as a slow-saturable absorber is still largely unexplored. Ultrafast

time-resolved measurements are also needed, as the excitation carrier dynamics plays an important role in the NLO performance, e.g., repetition rate and pulse duration in an ultrafast pulse laser [10]. The dependence of the exciton population on laser intensity and exciton–exciton annihilation was observed in a $MoSe_2$ monolayer by femtosecond transient absorption [11]. Ultrafast spectroscopic data show that the formation of trions in a $MoSe_2$ monolayer and the annihilation of trions followed a non-exponential decay [12,13]. However, the above reports do not answer the question of what role the relaxation of excited carriers plays in passive mode locking. Further research on the NLO properties of few-layer $MoSe_2$ as a slow-saturable absorber and the concurrent excited carrier relaxation processes is therefore required.

For a fiber laser with higher power and shorter pulse duration, it is necessary to have a deeper understanding of the NLO behavior of its mode-locking materials. In this work, we simultaneously studied the NLO responses and corresponding excitation carrier dynamics in liquid-phase-exfoliated $MoSe_2$ by *Z*-scan and degenerate pump-probe techniques. Our results show that few-layer $MoSe_2$ can be used as a slow-saturable absorber for passive mode locking. We employed a slow-absorber model modified from the Frantz–Nodvik equation to analyze this behavior and extract absorptive cross sections of the ground and excited states, NLO modulation depth, and saturated intensity of the few-layer $MoSe_2$. Our pump-probe results show that the decay of excited carriers in few-layer $MoSe_2$ follows two relaxations. A bi-exponential decay model was utilized to extract these two exact lifetimes to be ~2 ps and 218 ps, where the slow relaxation can be used to start the pulsed laser oscillation from continuous wave (CW) noise in the passive mode locking while the fast one stabilizes the mode locking for short pulses.

2. MATERIALS AND CHARACTERIZATIONS

We employed liquid-phase exfoliation techniques to prepare the 2D $MoSe_2$ dispersions in distilled water with sodium cholate (SC) as the surfactant [14]. Bulk $MoSe_2$ was dispersed into SC aqueous solution with 5 mg/mL and 10 mg/mL concentrations, respectively. A high-power sonic tip (Sonics VX-750) was employed to sonicate this dispersion for 90 min using 40% amplitude. To counter the temperature increase from sonication, we placed the vial holding the $MoSe_2$ dispersion into an ice water bath and set the sonic tip to pulse 2 s on and 4 s off. During sonication, the bulk $MoSe_2$ was exfoliated into a monolayer, bilayer, and few-layer flakes. To remove the large flakes, the sonicated dispersions were centrifuged at 2000 r/min for 90 min. The top half of the centrifuged dispersion was collected for characterizations. To study the dependence of NLO performance on the linear absorption, the obtained dispersion was diluted into two with different concentrations. Before the optical experiments, the geometry of the 2D $MoSe_2$ flakes was verified via transmission electron microscopy (TEM) and atomic force microscopy (AFM). No bulk $MoSe_2$ was found in the TEM images of the centrifuged dispersions. Figure 1(a) shows a typical few-layer nanoflake of $MoSe_2$ in TEM, where the stacking of monolayers can be clearly seen. We also found $MoSe_2$ monolayers in our dispersions, as shown in Fig. 1(b) in a high-resolution TEM image. Both TEM images imply the high quality of our $MoSe_2$ dispersion. These flakes are mainly composed of few-layer, bilayer, and monolayer $MoSe_2$. This is confirmed by Raman technique, which is a powerful tool to study the thickness of 2D materials. As indicated in Fig. 1(c), a strong peak located at ~241 cm^{-1} is originated from out-of-plane vibration (A_{1g}) [15]. We also observed two peaks at ~285 cm^{-1} and 353 cm^{-1}, which are assigned to

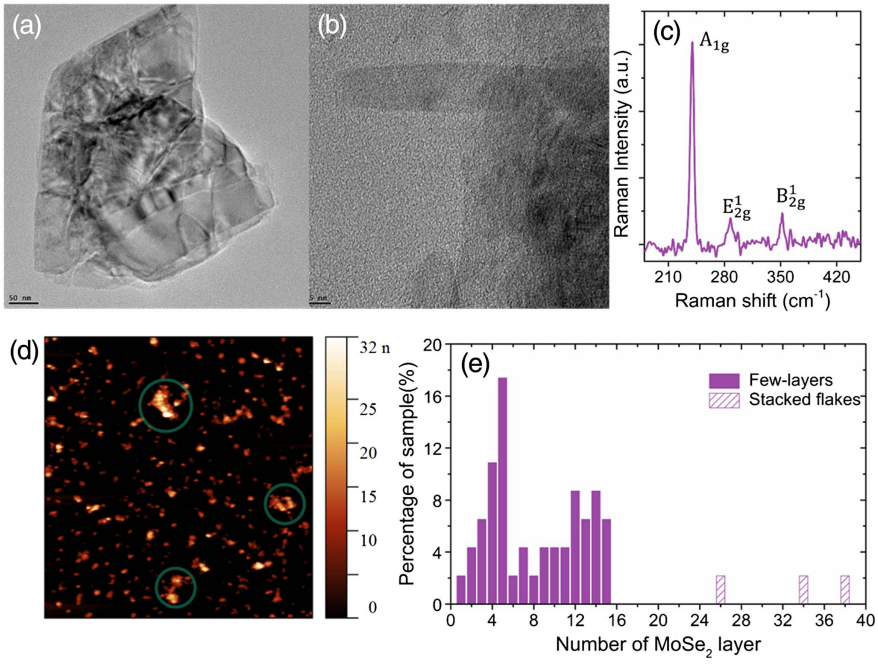

Fig. 1. TEM images showing (a) a few-layer $MoSe_2$ flake and (b) a monolayer $MoSe_2$ flake. The scale bar is 50 nm in (a) and 5 nm in (b). (c) Raman spectrum of the few-layer $MoSe_2$ flakes. (d) AFM image displaying the thickness of a large number of $MoSe_2$ flakes in a ~5 μm × 5 μm area. (e) Statistical thickness distribution of the $MoSe_2$ flakes in as-prepared dispersions.

the in-plane vibrations E^1_{2g} and B^1_{2g}, respectively. These peaks can be captured only in few-layer $MoSe_2$ instead of bulk [2]. To study the distribution of the number of the flake layers, AFM was employed to measure the sample. The AFM sample was prepared using the liquid-phase-exfoliated $MoSe_2$ dispersion before dilution. A drop of the dispersion was cast on a pre-cleaned silicon substrate, followed by a ~50°C vacuum treatment to evaporate the water. In a ~5 μm × 5 μm area shown in Fig. 1(d), a large number of $MoSe_2$ nano-flakes were seen. The thickness profiles were plotted using the AFM data to obtain the number of flake layers. Due to the ~0.67 nm thickness of a $MoSe_2$ monolayer [16], the number of layers in a flake with a thickness of L can be approximately calculated through dividing L by 0.67 nm. A statistical distribution of the number of flake layers was obtained, as shown in Fig. 1(e). It can be seen that most of the flakes in the centrifuged dispersion were less than 15 layers. From statistics, the layer number between 25 and 40 was also calculated, as seen in Fig. 1(e). It is likely to result from the stack of flakes, e.g., see the green circles in Fig. 1(e). Excluding these stacks in the estimates, flakes with between 3 and 15 layers account for more than 90% of the nanosheets in our dispersions.

3. NLO RESPONSE AND ULTRAFAST CARRIER DYNAMICS

Open-aperture Z-scan technique was utilized to study the NLO response of two $MoSe_2$ dispersions with linear absorption coefficients of 5.22 cm^{-1} and 6.51 cm^{-1}. To measure the linear absorption (A_0), we obtained the linear transmission (T_0) by measuring the transmitted intensity after the sample in a 1 mm thickness quartz cuvette and that after the same cuvette filled with deionized water. According to $A_0 = \alpha_0 l$, we can obtain the linear absorption coefficient, as indicated in the insets of Figs. 2(a) and 2(b). The Z-scan technique measures the transmission of the sample as a function of incident intensity. A varied intensity was obtained by moving the sample along the propagation direction, i.e., z direction, of a focused laser beam. The schematic of this optical setup is shown in Fig. 2(c). In order to eliminate the effect of laser fluctuations on our results, a small portion of the original laser beam was used as the reference signal. The laser pulses from the Ti: sapphire mode-locked laser (Coherent, RegA 9000) were at a wavelength of 800 nm, with a duration of ~100 fs and a repetition rate of 100 kHz. The solid scatter data points in Figs. 2(a) and 2(b) exhibit the experimental open-aperture Z-scan results of the $MoSe_2$ dispersions in 1 mm thickness quartz cuvettes. As the sample moves toward the focal point ($z = 0$ mm), a clear increase in the normalized transmission was observed. That is to say, the normalized transmission increases with the increase of the incident intensity, i.e., saturable absorption. The saturable absorption can be explained by Pauli-blocking [17]. The electrons are pumped to the conduction band from the valence band by absorbing incident photons. As the incident photon fluence increases, more electrons are occupying the conduction band until fully filled. The conduction band can then no longer accept more incoming electrons, which results in the transmission increase at higher incident light intensities.

The propagation equation describing how light attenuates in an NLO medium can be written as [18,19]

$$\frac{dI}{dz'} = -\alpha(I) \cdot I. \tag{1}$$

Here, I is the laser intensity, z' is the propagating distance in the material, and $\alpha(I) = \alpha_0 + \alpha_{NL} I$ represents the total absorption coefficients, including linear absorptive (α_0) and

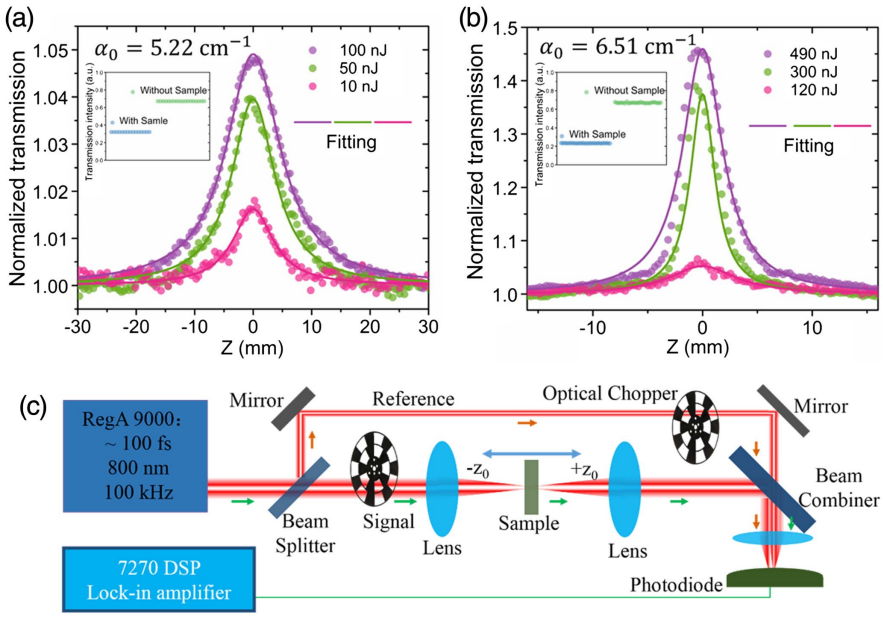

Fig. 2. Z-scan results of few-layer $MoSe_2$. The linear absorption coefficients are (a) 5.22 cm^{-1} and (b) 6.51 cm^{-1}, respectively, which are shown in the insets. The measurements were carried out under irradiation of increasing laser intensity. (c) Schematic of an open-aperture Z-scan. The laser pulses are at a center wavelength of 800 nm, with duration of ~100 fs and a repetition rate of 100 kHz from a Ti: sapphire mode-locked laser (Coherent, RegA 9000).

Table 1. NLO Performance of Few-Layer $MoSe_2$ Used as a Slow-Saturable Absorber

T_0 (%)	α_0 (cm^{-1})	α_{NL} (cm/GW)	$Im\chi^{(3)}$ (esu)	T_{max} (%)	ΔT (%)	A_{ns} (%)	I_S (MW/cm^2)	σ_e/σ_g
47.8	5.22	−0.017	-0.98×10^{-14}	55.2	7.4	44.8	39.37	0.81
34.9	6.51	−0.044	-2.50×10^{-14}	55.0	15.1	45.0	234.75	0.57

nonlinear absorptive (α_{NL}) parts. By employing Eq. (1) to fit the experimental Z-scan results (see the solid lines in Fig. 2), we obtained the nonlinear absorption coefficients of $MoSe_2$, which were calculated to be −0.017 cm/GW and −0.044 cm/GW for the samples with linear absorption coefficients of 5.22 cm^{-1} and 6.21 cm^{-1}, respectively. The more absorber atoms (larger linear absorption coefficient) that contribute to the nonlinear response, the larger the nonlinear coefficient is. Furthermore, the imaginary part of the third-order nonlinear optical susceptibility ($Im\chi^{(3)}$) can be calculated using $Im\chi^{(3)} = (\frac{10^{-7} c\lambda n^2}{96\pi^2})\alpha_{NL}$, where λ is the laser wavelength, c is the light speed, and n is the refractive index [20]. As shown in Table 1, $Im\chi^{(3)}$ of the few-layer $MoSe_2$ was estimated to be up to the order of 10^{-14} esu.

As the excited carrier dynamics is strongly relevant to the saturable absorption, we studied this relaxation process in $MoSe_2$ using a degenerate pump-probe technique. The schematic of this optical setup is plotted in the inset of Fig. 3(d). A train of intense laser pulses was employed as a pump to inject the excited electrons and holes into the valence and conduction bands of $MoSe_2$, respectively. Another train of pulses with relatively low intensity was delayed by a motorized linear translation stage as a probe. Both laser beams were at a wavelength of 800 nm, with a pulse duration of ~100 fs and a repetition rate of 100 kHz utilizing the same laser as before. An optical chopper was employed to modulate the probe and pump beams at 422 Hz and 733 Hz, respectively. The polarization of the probe beam was rotated by 90° with the help of a half-wave plate. This polarization orthogonality between pump and probe eliminated coherent spikes in all the pump-probe traces [21]. After the sample, the pump pulses were blocked by an aperture and a polarizer, while the probe pulses were corrected by a silicon photodiode and analyzed by an SR7270 DSP lock-in amplifier. The obtained differential transmission of $MoSe_2$, $\Delta T/T$, is plotted as scatter points in Fig. 3. It can be seen from Figs. 3(a) and 3(b) that the maximum differential transmission increases with the increase in the pump energies from 10 nJ to 200 nJ, which also implies saturable absorption. This is true for both few-layer $MoSe_2$ dispersions with different linear absorptions. Figures 3(c) and 3(d) plot the corresponding measurements at a long delay time, obviously showing a two-lifetime relaxation process. The bi-exponential decay processes of excited carrier were also observed in monolayer $MoSe_2$ [11].

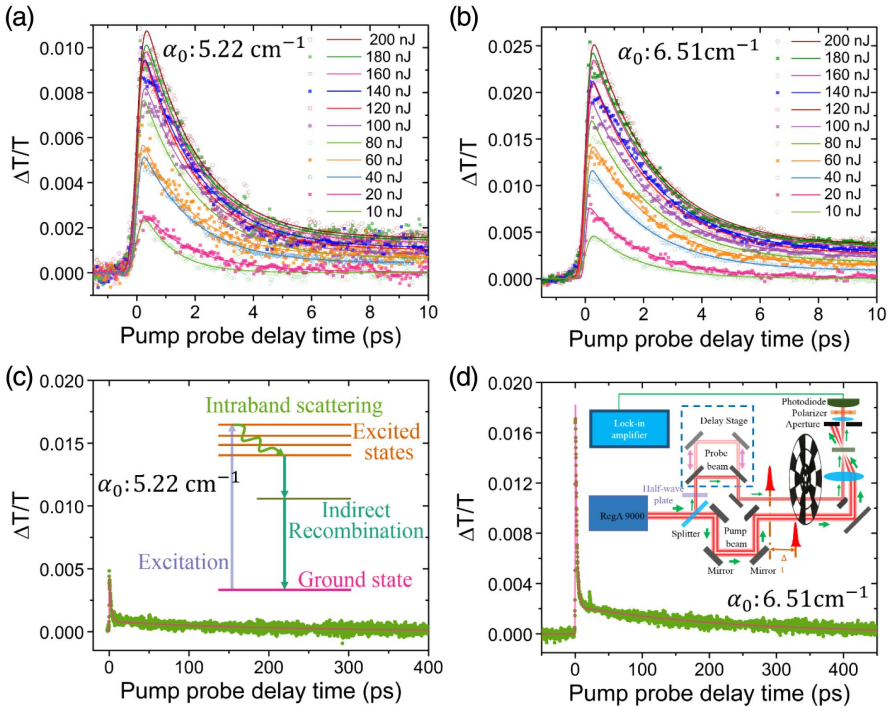

Fig. 3. Experimental (scatters) and fitting (solid lines) degenerate pump-probe traces of few-layer $MoSe_2$ based on an 800 nm laser with pulse duration of ~100 fs and repetition rate of 100 kHz. The inset in (c) shows the relaxation processes of the excited carriers. The inset in (d) shows degenerate pump-probe setup. An intense beam is employed to pump the materials, while another beam with relatively low intensity, which is delayed by a motorized linear translation stage, is used for probing the excited carriers. These two beams are modulated by an optical chopper at 733 Hz and 422 Hz, respectively. A half-wave plate and a polarizer are utilized to eliminate the coherent spikes.

Table 2. Fitting Parameters for the Experimental Differential Transmission of Two Few-Layer $MoSe_2$ Dispersions with the Linear Absorption Coefficients of 5.22 cm^{-1} and 6.51 cm^{-1}, Respectively

α_0 (cm^{-1})	D_1 (%)	D_2 (%)	τ_1 (ps)	τ_2 (ps)	σ (fs)
5.22	82.9	17.1	2.16	210.13	95
6.51	89.8	10.2	2.22	226.27	161

To obtain a deeper understanding of these relaxation processes, a bi-exponential equation with autocorrelations was utilized to model the experimental results [10,19]:

$$\frac{\Delta T}{T} = \left[D_1 \exp\left(-\frac{t}{\tau_1}\right)\mathrm{erfc}\left(\frac{\sigma}{\sqrt{2}\tau_1} - \frac{t}{\sqrt{2}\sigma}\right) + D_2 \exp\left(-\frac{t}{\tau_2}\right)\mathrm{erfc}\left(\frac{\sigma}{\sqrt{2}\tau_2} - \frac{t}{\sqrt{2}\sigma}\right)\right], \quad (2)$$

where D_1 and D_2 represent relative amplitudes, t is the pump-probe delay time, σ is the laser pulse width and "erfc" represents the standard error function. All the fittings are favorable to the experimental results, as the solid lines in Fig. 3. The fitting parameters are listed in Table 2. The corresponding relation processes are plotted in the inset of Fig. 3(c). At time zero, the carriers were excited by intense photons from the ground state to the excited state into a non-thermal equilibrium distribution. Within ~100 fs, these carriers were subsequently thermalized to a quasi-thermal equilibrium state. Since the time of this process is shorter than our laser pulse duration, it did not show in our results. Then the quasi-thermal carriers relaxed to a lower energy state via carrier–carrier scattering and/or phonon emission. This relaxation time was measured to be ~2.19 ps. Finally, the excited carrier annihilated via indirect recombination with a ~218.2 ps lifetime. This relaxation time is slightly smaller than that of the $MoSe_2$ monolayer (~300 ps), in which the optical transition is via direct band [22,23].

4. SLOW-SATURABLE ABSORPTION

Since both relaxations are much longer (~2 ps and ~218 ps) than the exciting laser pulse duration (~100 fs), the Z-scan results in Fig. 2 can be further analyzed using a slow-absorber model (SAM) modified from the Frantz–Nodvik equation in the following [24]:

$$T(F) = T_0 + \frac{T_{\mathrm{FN}} - T_0}{1 - T_0}(T_{\max} - T_0). \quad (3)$$

Here, $T_0 = e^{-\sigma_g NL}$ is the linear transmission, $T_{\max} = e^{-\sigma_e NL}$ is the saturable transmission, and $T_{\mathrm{FN}} = \ln[1 + T_0(e^{\frac{\sigma_g F}{\hbar\omega}} - 1)]/(\sigma_g F/\hbar\omega)$. σ_g and σ_e represent the absorptive cross sections of ground and excited states, respectively. N represents the density of the absorptive centers (density of atoms for approximation), and $L = 1$ mm is the sample thickness. ω is the angular frequency of the incident photons. The results are shown in Fig. 4(a). The corresponding NLO parameters are listed in Table 1. The non-saturable absorption loss can be calculated via $A_{\mathrm{ns}} = 1 - T_{\max}$ to be 44.8% and 45.0% with corresponding coefficients for the dispersions with linear absorption coefficients of 5.22 cm^{-1} and 6.51 cm^{-1}, respectively. The modulation depth, ΔT, defined as the difference between the maximum and minimum transmissions, i.e., $\Delta T = T_{\max} - T_0$, is shown in Fig. 4(a) as well. For the few-layer $MoSe_2$ dispersions with linear transmission of 47.8% and 34.9%, ΔT is measured to be 7.4% and 20.0%, respectively. It implies that the NLO modulation depth can be controlled by changing the linear absorption of the dispersion, which can be tuned by diluting or concentrating a sample. This difference is more obvious when the transmission is converted to the differential absorption, as shown in Fig. 4(b). Another important NLO parameter is the saturated intensity I_S, which refers to the laser intensity at the half NLO modulation depth of a saturable absorber. The I_S was fitted to be 39.37 MW/cm^2 and 234.75 MW/cm^2 for the two samples with linear absorptions of 5.22 cm^{-1} and 6.51 cm^{-1}, respectively. Combining the result in Ref. [1] of I_S = ~590 MW/cm^2 for a sample with a linear absorption of 7.93 cm^{-1}, we can see that the saturable intensity increases with the linear absorption. This is because more photons are needed to saturate an absorber with higher concentration of carriers. The ratios of absorption cross sections of excited states to ground states, σ_e/σ_g, were estimated to be 0.81 and 0.57 for the 47.8% and 34.9% transmission few-layer $MoSe_2$, respectively. This is in agreement with other saturable absorption materials: the absorptive cross section of the excited state is smaller than that of the ground state [10,19,20,25]. The small σ_e/σ_g also indicates low non-saturable absorption of few-layer $MoSe_2$ when it is working for passive mode locking.

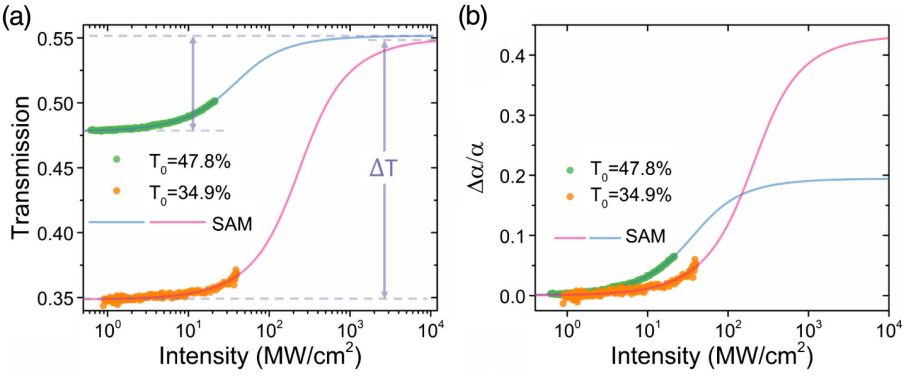

Fig. 4. NLO performance of few-layer-$MoSe_2$ analyzed by a slow-saturable absorber model. (a) Experimental (scatters) and fitting (solid lines) transmission as a function of intensity. (b) Corresponding differential absorption converted from (a).

5. CONCLUSION

In this work, we studied the NLO properties of few-layer $MoSe_2$ using open-aperture Z-scan and degenerate pump-probe techniques based on an 800 nm femtosecond laser. The results reported in this work indicate that few-layer $MoSe_2$ dispersions possess saturable absorption with an imaginary part of the third-order NLO susceptibility of $\sim 10^{-14}$ esu. The analysis based on the slow-absorber model shows that the saturated intensities of few-layer $MoSe_2$ are 39.37 MW/cm^2 and 234.75 MW/cm^2 for the linear absorption coefficients of 5.22 cm^{-1} and 6.51 cm^{-1}, respectively, with a corresponding NLO modulation depth of 7.4% and 15.1%. The pump-probe results indicate that the excited-carrier relaxation in $MoSe_2$ is composed of a bi-exponential process with lifetimes ~2 ps and ~218 ps, respectively. These two lifetimes may be attributed to carrier–carrier scattering and indirect recombination. As in graphene, this two-lifetime relaxation indicates $MoSe_2$ as a promising material for passive mode locking to produce ultrashort laser pulses, where the slow relaxation facilitates the starting of pulsed laser oscillation from CW noise, while the fast one stabilizes the mode locking for short pulses.

Funding. Science Foundation Ireland (SFI) (12/IA/1306); Seventh Framework Programme (FP7) (ISLA project no. 287732); National Natural Science Foundation of China (NSFC) (61522510, 61675217, 11704261, 11575118); Strategic Priority Research Program of Chinese Academy of Sciences (CAS) (XDB16030700); Key Research Program of Frontier Science of Chinese Academy of Sciences (QYZDB-SSW-JSC041); the Program of Shanghai Academic Research Leader (17XD1403900); Shenzhen Key Lab Fund (ZDSYS 20170228105421966).

Acknowledgment. G. Wang, K. Wang, A. A. Baker-Murray, and W. J. Blau thank the Science Foundation Ireland and European Commission under the Seventh Framework Programme. J. Wang acknowledges the NSFC grant, the Strategic Priority Research Program of CAS, the Key Research Program of Frontier Science of CAS, and the Program of Shanghai Academic Research Leader. P. Fan, J. T. Luo, and G. Liang thank the Shenzhen Key Lab Fund. We are grateful for the support of materials from Dr. Chuanfang Zhang and the discussions with Brian Jennings.

[†]These authors contributed equally to this work.

REFERENCES

1. K. Wang, Y. Feng, C. Chang, J. Zhan, C. Wang, Q. Zhao, J. N. Coleman, L. Zhang, W. J. Blau, and J. Wang, "Broadband ultrafast nonlinear absorption and nonlinear refraction of layered molybdenum dichalcogenide semiconductors," Nanoscale **6**, 10530–10535 (2014).
2. P. Tonndorf, R. Schmidt, P. Böttger, X. Zhang, J. Börner, A. Liebig, M. Albrecht, C. Kloc, O. Gordan, and D. R. Zahn, "Photoluminescence emission and Raman response of monolayer MoS_2, $MoSe_2$, and WSe_2," Opt. Express **21**, 4908–4916 (2013).
3. S. Tongay, J. Zhou, C. Ataca, K. Lo, T. S. Matthews, J. Li, J. C. Grossman, and J. Wu, "Thermally driven crossover from indirect toward direct bandgap in 2D semiconductors: $MoSe_2$ versus MoS_2," Nano Lett. **12**, 5576–5580 (2012).
4. G. Wang, S. Zhang, X. Zhang, L. Zhang, Y. Cheng, D. Fox, H. Zhang, J. N. Coleman, W. J. Blau, and J. Wang, "Tunable nonlinear refractive index of two-dimensional MoS_2, WS_2, and $MoSe_2$ nanosheet dispersions," Photon. Res. **3**, A51–A55 (2015).
5. Z. Luo, D. Wu, B. Xu, H. Xu, Z. Cai, J. Peng, J. Weng, S. Xu, C. Zhu, and F. Wang, "Two-dimensional material-based saturable absorbers: towards compact visible-wavelength all-fiber pulsed lasers," Nanoscale **8**, 1066–1072 (2016).
6. R. Sharma, J. Aneesh, R. K. Yadav, S. Sanda, A. Barik, A. K. Mishra, T. K. Maji, D. Karmakar, and K. Adarsh, "Strong interlayer coupling mediated giant two-photon absorption in $MoSe_2$/graphene oxide heterostructure: quenching of exciton bands," Phys. Rev. B **93**, 155433 (2016).
7. J. R. Schaibley, T. Karin, H. Yu, J. S. Ross, P. Rivera, A. M. Jones, M. E. Scott, J. Yan, D. Mandrus, and W. Yao, "Population pulsation resonances of excitons in monolayer $MoSe_2$ with sub-1 μeV linewidths," Phys. Rev. Lett. **114**, 137402 (2015).
8. N. Dong, Y. Li, Y. Feng, S. Zhang, X. Zhang, C. Chang, J. Fan, L. Zhang, and J. Wang, "Optical limiting and theoretical modelling of layered transition metal dichalcogenide nanosheets," Sci. Rep. **5**, 14646 (2015).
9. J. Koo, J. Park, J. Lee, Y. M. Jhon, and J. H. Lee, "Femtosecond harmonic mode-locking of a fiber laser at 3.27 GHz using a bulk-like, $MoSe_2$-based saturable absorber," Opt. Express **24**, 10575–10589 (2016).
10. G. Wang, K. Wang, B. M. Szydłowska, A. A. Baker-Murray, J. J. Wang, Y. Feng, X. Zhang, J. Wang, and W. J. Blau, "Ultrafast nonlinear optical properties of a graphene saturable mirror in the 2 μm wavelength region," Laser Photon. Rev. **11**, 1700166 (2017).
11. N. Kumar, Q. Cui, F. Ceballos, D. He, Y. Wang, and H. Zhao, "Exciton-exciton annihilation in $MoSe_2$ monolayers," Phys. Rev. B **89**, 125427 (2014).
12. F. Gao, Y. Gong, M. Titze, R. Almeida, P. M. Ajayan, and H. Li, "Valley trion dynamics in monolayer $MoSe_2$," Phys. Rev. B **94**, 245413 (2016).
13. A. Singh, G. Moody, S. Wu, Y. Wu, N. J. Ghimire, J. Yan, D. G. Mandrus, X. Xu, and X. Li, "Coherent electronic coupling in atomically thin $MoSe_2$," Phys. Rev. Lett. **112**, 216804 (2014).
14. J. N. Coleman, M. Lotya, A. O'Neill, S. D. Bergin, P. J. King, U. Khan, K. Young, A. Gaucher, S. De, and R. J. Smith, "Two-dimensional nanosheets produced by liquid exfoliation of layered materials," Science **331**, 568–571 (2011).
15. Y. Ding, Y. Wang, J. Ni, L. Shi, S. Shi, and W. Tang, "First principles study of structural, vibrational and electronic properties of graphene-like MX_2 (M = Mo, Nb, W, Ta; X = S, Se, Te) monolayers," Physica B **406**, 2254–2260 (2011).
16. J. C. Shaw, H. Zhou, Y. Chen, N. O. Weiss, Y. Liu, Y. Huang, and X. Duan, "Chemical vapor deposition growth of monolayer $MoSe_2$ nanosheets," Nano Res. **7**, 511–517 (2014).
17. Q. Bao, H. Zhang, Y. Wang, Z. Ni, Y. Yan, Z. X. Shen, K. P. Loh, and D. Y. Tang, "Atomic-layer graphene as a saturable absorber for ultrafast pulsed lasers," Adv. Funct. Mater. **19**, 3077–3083 (2009).
18. Y. Feng, N. Dong, G. Wang, Y. Li, S. Zhang, K. Wang, L. Zhang, W. J. Blau, and J. Wang, "Saturable absorption behavior of free-standing graphene polymer composite films over broad wavelength and time ranges," Opt. Express **23**, 559–569 (2015).
19. K. Wang, B. M. Szydłowska, G. Wang, X. Zhang, J. J. Wang, J. J. Magan, L. Zhang, J. N. Coleman, J. Wang, and W. J. Blau, "Ultrafast nonlinear excitation dynamics of black phosphorus nanosheets from visible to mid-infrared," ACS Nano **10**, 6923–6932 (2016).
20. K. Wang, J. Wang, J. Fan, M. Lotya, A. O'Neill, D. Fox, Y. Feng, X. Zhang, B. Jiang, and Q. Zhao, "Ultrafast saturable absorption of two-dimensional MoS_2 nanosheets," ACS Nano **7**, 9260–9267 (2013).
21. C. Luo, Y. Wang, F. Chen, H. Shih, and T. Kobayashi, "Eliminate coherence spike in reflection-type pump-probe measurements," Opt. Express **17**, 11321–11327 (2009).
22. Z. Nie, C. Trovatello, E. A. Pogna, S. Dal Conte, P. B. Miranda, E. Kelleher, C. Zhu, I. C. E. Turcu, Y. Xu, and K. Liu, "Broadband nonlinear optical response of monolayer $MoSe_2$ under ultrafast excitation," Appl. Phys. Lett. **112**, 031108 (2018).

23. C. Trovatello, Z. Nie, E. A. A. Pogna, S. D. Conte, P. Miranda, G. Cerullo, and F. Wang, "Ultrafast characterization of saturable absorption in monolayer $MoSe_2$," in *Graphene*, Barcelona, Spain (2017).
24. Z. Burshtein, P. Blau, Y. Kalisky, Y. Shimony, and M. Kikta, "Excited-state absorption studies of Cr^{4+} ions in several garnet host crystals," IEEE J. Quantum Electron. **34**, 292–299 (1998).
25. J. Huang, N. Dong, S. Zhang, Z. Sun, W. Zhang, and J. Wang, "Nonlinear absorption induced transparency and optical limiting of black phosphorus nanosheets," ACS Photon. **4**, 3063–3070 (2017).